



The effect of reactants adsorption and products desorption for Au/TiO₂ in catalyzing CO oxidation

Shuai Wei ^a, Wei-Wei Wang ^{a,*}, Xin-Pu Fu ^a, Shan-Qing Li ^{b,*}, Chun-Jiang Jia ^{a,*}

^a Key Laboratory for Colloid and Interface Chemistry, Key Laboratory of Special Aggregated Materials, School of Chemistry and Chemical Engineering, Shandong University, Jinan 250100, China

^b Department of Chemistry and Materials Engineering, Chizhou University, Chizhou 247000, China



ARTICLE INFO

Article history:

Received 27 January 2019

Revised 7 May 2019

Accepted 23 June 2019

Available online 17 July 2019

Keywords:

Au/TiO₂

In-situ characterization

Reactants adsorption

Products desorption

CO oxidation

ABSTRACT

Supported gold catalysts exhibit very high activity for CO oxidation. However, there is lack of systematic study for supports effect on reactants adsorption and products desorption. Herein, we successfully prepared supported gold catalysts on TiO₂ matrix exposing either {1 0 1} or {0 0 1} crystal plane (labeled as Au/TiO₂-1 0 1 and Au/TiO₂-0 0 1 respectively) by deposition-precipitation (DP) method. It is found that the reactivity of Au/TiO₂-1 0 1 was much higher than Au/TiO₂-0 0 1 in CO oxidation reaction (9.33×10^{-3} mol_{CO}_{gAu⁻¹} s⁻¹ vs. 6.23×10^{-4} mol_{CO}_{gAu⁻¹} s⁻¹ at 30 °C). The gold nanoparticles (~2 nm) were detected as sole gold species in Au/TiO₂-1 0 1, while not only gold nanoparticles (~4 nm) but also clusters (~1.3 nm) were present in Au/TiO₂-0 0 1. The difference in gold status induced different CO adsorption situations that CO was more effectively adsorbed on gold nanoparticles in Au/TiO₂-1 0 1 which existed more Au⁰ site. Meanwhile, we revealed that the bidentate carbonate, which could either block active sites for the reaction or hinder access of reactants, were adsorbed much more strongly on TiO₂-0 0 1. While on TiO₂-1 0 1, bicarbonate was the main surface species which was easier decomposed to form CO₂. Therefore, the differences between Au/TiO₂-1 0 1 and Au/TiO₂-0 0 1 in the efficiency of CO adsorption and the ability of CO₂ desorption resulted in disparate reactivity. We reasonably gave the deep insight into the support effect that was intrinsically related to the adsorption and desorption behavior of surface species on the catalyst.

© 2019 Elsevier Inc. All rights reserved.

1. Introduction

Supported gold catalysts have drawn tremendous attention in research [1,2], since the breakthrough of the extremely high activity of that in catalyzing CO oxidation at low temperature by Haruta and co-workers in the 1980s [3]. Recently, plenty of researches have been focused on the source of the remarkable catalytic behavior from supported gold catalysts [4–8]. There are three important factors shown significant influence for the reactivity of supported gold catalysts during catalyzing CO oxidation, the components and size of gold species [7,9], the properties of support material [10,11], as well as the interaction between metal and support [12,13]. Despite of the deep study on the factors which influence the reactivity of supported gold catalysts, there are still controversies because of the complexity of the catalytic system.

Furthermore, it is more difficult to study the impact on reactants adsorption and products desorption due to the intertwined above factors.

Both CO adsorption and CO₂ desorption for supported gold catalysts were related to the activity in catalyzing CO oxidation reaction [7,8,12,14,15]. The CO adsorption on metal oxide as support was merely occurred at ultralow temperatures, so the carrier's adsorption of CO contributes negligibly to the activity at room temperature [6,16]. While, the interaction between gold and supports strongly influenced the status of gold [11,12], and the state of gold directly affected the adsorption of CO, thereby affecting the activity [7,8,12]. As for products desorption, it was mainly influenced by the interaction between CO₂ and supports [14]. In addition, the carbonate species were formed by adsorption CO₂ on the catalysts surface [15,17,18], and the carbonate species could block the active sites or prevent reactants approaching that site. Therefore, the properties of supports extremely affected the ability of CO adsorption and CO₂ desorption for the supported catalysts thus leading to various reactivity.

* Corresponding authors.

E-mail addresses: wangww@sdu.edu.cn (W.-W. Wang), shanqingli@czu.edu.cn (S.-Q. Li), jiacj@sdu.edu.cn (C.-J. Jia).

Various metal oxides, including TiO_2 [12], CeO_2 [7], ZrO_2 [19], MgO [20], Fe_2O_3 [21], and Co_3O_4 [22], were considered as Au supports, for the purposes of obtaining high reactivity. Due to different physical and chemical properties, different supports differed the ability of activation the reactants as well as the reaction pathways for supported catalysts [23,24]. However, supported gold catalysts with different matrixes were not comparable owing to the complexity of the system. Thus some research focused on supported gold on same matrixes exposed different crystal plane valued as catalysts [25–28]. The matrixes with different facet show the same chemical composition but different surface and electronic structures [29–31], which was a good system for exploring carrier effects [25–28]. Flytzani-Stephanopoulos et al. indicated that gold nanoparticles supported on ceria nanorod ($\{1\ 1\ 0\}$ and $\{1\ 0\ 0\}$) showed much higher reactivity for water-gas shift (WGS) reaction than on CeO_2 exposed other crystal planes, attributed to the more active for gold stabilization/activation on CeO_2 nanorod [25]. Ma et al. digged out that $\text{Au}/\text{Co}_3\text{O}_4\text{-}\{1\ 1\ 0\}$ exhibit the maximum amount of oxygen vacancies than $\text{Au}/\text{Co}_3\text{O}_4\text{-}\{0\ 1\ 1\}$ and $\text{Au}/\text{Co}_3\text{O}_4\text{-}\{0\ 0\ 1\}$, resulting in highest reactivity of ethylene oxidation [26]. Furthermore, TiO_2 also has attracted a lot of research as a common redox carrier [32–35]. Liu et al. found that the chemical oscillations were depended on the crystal planes of titanium dioxide nanocrystals during alternate H_2 and O_2 pretreatments on gold-titania catalysts which varied reactivity for CO oxidation [27]. In addition, they also demonstrated that the crystal planes of the titania in gold-titania system greatly influenced the ability of O_2 activation in CO oxidation reaction [28]. Huang et al. indicated that dual-perimeter-sites catalysis in low temperature CO oxidation reaction was strongly influenced by the crystal plane of support because the migration of CO molecules was depended on the activity of $\text{Au}-\text{TiO}_2$ perimeter sites [35].

Even though comprehensive researches have been studied to explore the effect of supports with different crystal plane, there is hardly mentioned the impact of reactants adsorption and products desorption for the catalytic CO oxidation reaction. Therefore, in this paper, we chose two types of anatase TiO_2 exposed $\{1\ 0\ 1\}$ and $\{0\ 0\ 1\}$ crystal plane as supports and prepared Au/TiO_2 catalysts by deposition-precipitation method (labeled as $\text{Au}/\text{TiO}_2\text{-}x$, $x = 1\ 0\ 1$, $0\ 0\ 1$). The effects of reactants adsorption and products desorption for these two catalysts in catalyzing CO oxidation reaction were revealed. Based on TEM and *in-situ* DRIFTS, the different size distribution of gold nanoparticles on these two catalysts indicated the distinct interaction between metal and support, therefore, leading to the difference in effective CO adsorption further influencing the reactivity. Moreover, when CO_2 was produced during reaction, carbonate species were appeared and it was more tightly adsorbed on $\text{TiO}_2\text{-}0\ 0\ 1$ than that on $\text{TiO}_2\text{-}1\ 0\ 1$, which may block the active site. The finding greatly advances the fundamental understanding of the reactants adsorption and products desorption effect of gold-titania catalysts for catalyzing CO oxidation.

2. Experimental

2.1. Synthesis of TiO_2 nanocrystals with $\{1\ 0\ 1\}$ and $\{0\ 0\ 1\}$ planes exposed

2.1.1. Synthesis of Ti(OH)_4 precursor [36]

Briefly, the solution of TiCl_4 (6.6 mL) was added dropwise to the 20 mL of HCl (0.43 mol/L) aqueous solution in an ice bath under stirring. This clear solution of TiCl_4 was then added to aqueous $\text{NH}_3\text{-H}_2\text{O}$ (50 mL, 5.5 wt%). Afterward, the other aqueous $\text{NH}_3\text{-H}_2\text{O}$ (4 wt%) was added until the pH reached neutral value. The suspension was then aged, centrifuged, washed and finally dried at 80 °C for 6 h.

2.1.2. Synthesis of $\text{TiO}_2\text{-}1\ 0\ 1$ nanocrystals [36]

Firstly, NH_4Cl (0.2 g) was dissolved in a mixed solution of isopropyl alcohol (15 mL) and ultrapure water (18.2 MΩ, 15 mL) in a Teflon bottle (100 mL). Then the as-prepared Ti(OH)_4 (2.0 g) was added into the above mixture under stirring. The Teflon bottle was then put in a autoclave and kept at 180 °C for 24 h. After the reaction, the products were centrifuged, washed and finally dried at 80 °C for 6 h.

2.1.3. Synthesis of $\text{TiO}_2\text{-}0\ 0\ 1$ nanocrystals [37]

$\text{TiO}_2\text{-}0\ 0\ 1$ was prepared by the hydrothermal method. Typically, Ti(OBu)_4 (TBOT, 25 mL) were added into a Teflon bottle (100 mL). Then HF solution (3 mL, 40 wt%) were added dropwise and stirred for another 1 h. The Teflon bottle was put in a autoclave and kept at 180 °C for 24 h. After the reaction, the products were separated by centrifugation and washed. Thereafter, these as-obtained products were dried in air at 80 °C for 6 h. The powder was dispersed in NaOH (500 mL, 0.1 M) aqueous and stirred for 24 h to remove fluorine. Finally, they were centrifuged, washed, and dried in air at 80 °C for 6 h.

2.2. Preparation of gold-titanium catalysts

The Au/TiO_2 catalysts with 1 wt% Au loading were prepared by deposition-precipitation method [7,8]. Firstly, TiO_2 support (0.5 g) was dispersed in ultrapure water (18.2 MΩ, 25 mL). Then the ammonium carbonate (1.2 g, 12.5 mL) was added into the suspension under stirring, followed by dropping the $\text{HAuCl}_4\text{-3H}_2\text{O}$ aqueous solution (0.0125 M, 2 mL). After stirring for 20 min and aging for 1 h. The products were filtered, washed and finally dried at 75 °C for 3 h. The samples were activated with air (30 $\text{mL}\cdot\text{min}^{-1}$) at 300 °C for 0.5 h in the subsequent characterization, labeled as Au/TiO_2 activated.

2.3. Characterization of the catalysts

Inductively coupled plasma atom emission spectroscopy (ICP-AES) analysis was conducted on a Perkin-Elmer 3300DV emission spectrometer, which was in order to measure the gold loading in the gold-titanium catalysts.

Transmission electron microscopy (TEM) and high-angle annular dark-field scanning TEM (HAADF-STEM) were carried out on a JEM-2100F (JEOL) instrument under 200 kV. The ultra-thin carbon film-coated copper grid was used to prepare the samples.

The X-ray diffraction (XRD) pattern for catalyst was collected on PANalytical X'pert3 powder diffractometer (40 kV, 40 mA, $\lambda_{\text{Cu-K}\alpha} = 0.15418 \text{ nm}$) with measurement range of 10–90° and gathering time of 8.5 min.

X-ray photoelectron spectroscopy (XPS) was conducted on Axis Ultra XPS spectrometer (Al K α radiator). The C 1s peak energy at 284.8 eV was used to calibrate the binding energies for all measured catalysts.

The HORIBA Jobin Yvon spectrometer with an excitation wavelength of 632 nm was used to collect the Raman spectra. The spectral resolution was 2 cm^{-1} and the measurement range was set from 50 to 800 cm^{-1} . The TOPS Micro Raman *in-situ* reactor was equipped to collect the *in-situ* Raman spectra. The samples were firstly activated in air (flow rate, 30 $\text{mL}\cdot\text{min}^{-1}$, 300 °C/30 min) followed by N_2 purging and cooling down to 30 °C. Then the continuous spectra were collected after switching to reaction gas atmosphere (1%CO/20%O₂/N₂) with each lasting for 10 min.

In-situ DRIFTS-MS was carried on a Bruker Vertex 70 FTIR spectrometer combined with mass spectrum (LC-D200M PRO, TILON). The DRIFTS was fitted with a mercury-cadmium-telluride (MCT) detector and the sample cell was equipped with CaF₂ windows. For the purpose of decreasing dead volume when changing the

various gases, one electro-control quick switching system was used. About 20 mg samples were firstly activated in air (flow rate, 30 mL·min⁻¹, 300 °C/30 min) followed by He purging and cooling down to 30 °C. Then three types of *in-situ* DRIFTS tests were performed at 30 °C: CO adsorption-desorption mode, steady-state mode and CO₂ adsorption-desorption mode. For the CO adsorption-desorption mode, the gas were changed in this order: 2%CO/He, He, 2%CO/He, 5%O₂/He. And each gas passed through the catalysts for 30 min. For steady-state experiment, the reaction gas atmosphere (1%CO/20%O₂/N₂, 30 mL/min) were constantly fed through the catalysts for 4 h. For CO₂ adsorption-desorption mode, 2%CO₂/N₂ was firstly fed through the catalysts for 30 min and followed by N₂ purging. The scanning range for IR spectra was 4000 cm⁻¹ to 1000 cm⁻¹ and the resolution for the spectra was 4 cm⁻¹. The spectra collected in He or N₂ before test were chosen as background.

The temperature-programmed reduction test of CO (CO-TPR) was performed in apparatus equipped with six-way valve for avoiding dead volume and residual air. The end gas was online monitored by one mass spectrometer in real-time. The catalysts were firstly activated in pure O₂ at 300 °C for 30 min. Under the atmosphere of 2%CO/N₂, the temperature was ramped from 30 °C to 300 °C (10 °C·min⁻¹). For temperature programmed desorption measurements of CO₂ (CO₂-TPD), the catalysts were activated in pure O₂ at 300 °C for 0.5 h. Then CO₂ (30 mL/min) was fed in at room temperature for 30 min and subsequently purged with pure He (30 mL/min). Desorption curves were acquired under pure He atmosphere (30 mL/min) by heating the catalyst from 30 °C to 300 °C (10 °C·min⁻¹). The CO-TPR and CO₂-TPD curves were recorded by mass spectrum (LC-D200M, TILON) with *m/z* = 28 (N₂ or CO), 44 (CO₂).

2.4. Catalytic tests and kinetics measurement

The reactivity of Au/TiO₂catalysts in catalyzing CO oxidation reaction was tested in a fixed-bed flow reactor under a gas mixture of 1%CO/20%O₂/N₂ (67 mL·min⁻¹, Deyang Gas Company, Jinan, 99.997% purity). Before reaction, 20 mg catalysts were activated at 300 °C for 0.5 h in air (21%O₂/N₂). After activation, the catalysts were cooled down under pure N₂. For light-off catalytic test, the reactant gas was fed in and the catalysts temperature was ramped (3 °C/min) from room temperature to 300 °C. The steady-state test was performed in the reactant gas at designated temperature (ca. 30 °C or 0 °C) for 12 h. The infrared gas analyzer (Gasboard-3500, Wuhan Sifang Company, China) were used online to quantify the constitution of CO and CO₂ in outlet gas.

The apparent activation energy (Ea). For both catalysts, the Ea was measured with the same reactor for catalytic performance above. Appropriate amount of catalysts diluted with SiO₂ (the corresponding height was less than 8 mm) were used in the kinetics experiments. The experiments were carried out by changing temperature and gas flow rate, with conversion between 5% and 15%. The product gas was measured by the infrared gas analyzer (Gasboard-3500, Wuhan Sifang Company, Wuhan, China).

2.5. First-principles calculations

Spin-polarized density functional theory (DFT) calculations were carried out using the Vienna Ab initio Simulation Package [38–41]. The geometric structures were optimized within the Perdew-Burke-Ernzerhof (PBE) exchange-correlation functional as well as the projector augmented wave method (PAW) [41–43]. In order to estimate the strong on-site interaction of localized electrons, a Hubbard U term (DFT + U) was involved in the first-principle computations, and the value of U was scaled to 4.0 eV in accordance with previous researches [44,45]. The cut-off energy

for plane wave basis was set to 400 eV. The convergence threshold of the electronic self-consistency was specified to 0.01 meV, and the total energy change between two ionic relaxation steps was designated 0.02 eV. The cleaved TiO₂ {0 0 1} surface was comprised of a five-layer slab as well as a vacuum layer of 15 Å. The Brillouin zone of the constructed (3 × 3) supercell (135 atoms) was sampled with the k-points (2 × 2 × 1). Analogously, the Brillouin zone of constructed TiO₂ {1 0 1} (1 × 4) supercell (144 atoms) was sampled with the k-points (2 × 2 × 1). The interaction between TiO₂ and Au was simulated with Au₁₁ (two layers) lying on the TiO₂ surface. The selective dynamics and conjugate gradient algorithm were used to calculate Γ-point vibrational frequencies.

3. Results and discussion

3.1. Morphological and structural characterizations

As shown in the TEM images (Fig. S1), octahedrons and sheets geometrically shaped TiO₂ nanocrystals with primarily exposed surface {1 0 1} and {0 0 1}, labeled as TiO₂-1 0 1 and TiO₂-0 0 1, were prepared respectively, in agreement with previous studies of titania nanomaterials [36,37]. Determined from the XRD results (Fig. S2a), both the diffracted patterns could be indexed to the anatase structures (tetragonal, I4₁/amd, JCPDS no. 01-089-4921). Notably, compared with two supports, the half-maximum of anatase TiO₂ (0 0 4) diffraction peaks centered at 37.8° was much broader for TiO₂-0 0 1 than that for TiO₂-1 0 1, which indicated that the TiO₂ sheets were thinner than that of TiO₂ octahedrons in the [0 0 1] direction [46]. The intensity of the (2 0 0) diffraction peaks centered at 48° was much higher and narrower for TiO₂-0 0 1 than that for TiO₂-1 0 1, which proved that the TiO₂ sheets had longer side length in the [1 0 0] direction than TiO₂ octahedrons [46]. Here, two TiO₂ materials with primarily exposed surface {1 0 1} and {0 0 1} were successfully prepared and can be utilized as good model supports to deposit gold further to study the reactants adsorption and products desorption effect for gold catalysis.

After depositing gold species by the same deposition-precipitation method (Fig. S3), no obvious Au nanoparticles were observed in these two catalysts, which indicating ultra-small size of Au species in the fresh samples. However, the size distribution of the Au species was greatly affected by different lattice plane after activation (Fig. 1 and Fig. S4). The size distribution was narrow with an average size of 2.2 nm for gold particles in the Au/TiO₂-1 0 1 sample, while clustered gold species in sub-nanometer size were scarcely detected. However, for the Au/TiO₂-0 0 1 catalyst, in addition to few detectable gold particles with diameter of ~4 nm, abundant ultra-small sized gold clusters with average diameter of 1.3 nm were clearly evidenced in the HAADF-STEM image (Fig. 1e and Fig. S4). It could be proved by XPS (Fig. S5) that the gold species in activated Au/TiO₂-0 0 1 and Au/TiO₂-1 0 1 were metallic with the Au 4f_{3/2} peak centered at 83.3 eV [8,47], which was consistent with H₂-TPR results (Fig. S6). The intensity of Au 4f peak for Au/TiO₂-0 0 1 was lower than that for Au/TiO₂-1 0 1 (Fig. S5) because of a lower surface-to-bulk ratio of Au nanoparticles [35]. The aggregate states of gold species were strongly influenced by the bonding strength with the surface properties of TiO₂, such as surface oxygen vacancies and surface energy. On one hand, TiO₂-1 0 1 exposes under-coordinated five-fold Ti (Ti_{5c}) and twofold O (O_{2c}, or O_{br}), as well as fully coordinated six-fold Ti_{6c} and three-fold O_{3c} ions, and is very stable and inert with the lowest surface energy of ~0.43 J/m² [29,30]. On the other hand, TiO₂-0 0 1 had much higher surface energy (~0.90 J/m²) resulted in a (1 × 4) reconstruction [30,31]. The huge difference between two crystal planes could differ in the existence state of gold.

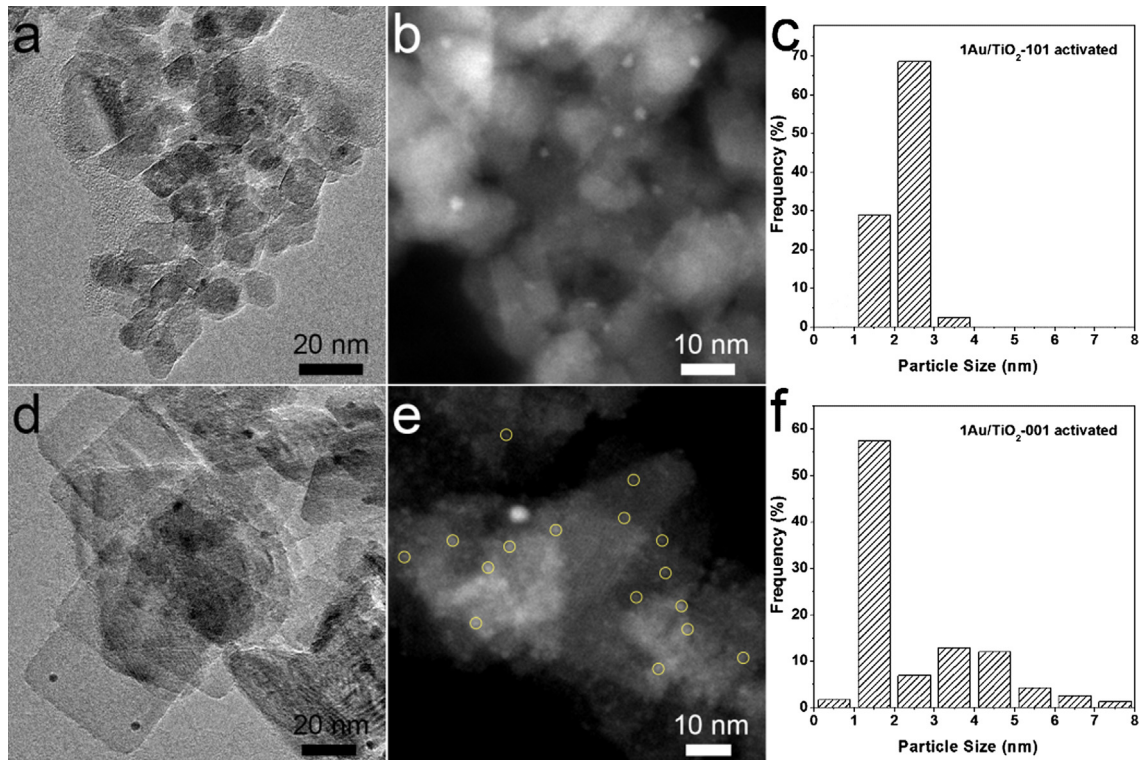


Fig. 1. TEM (a and d) and HAADF-STEM (b and e) images and size distribution (c and f) for the activated Au/TiO₂-1 0 1 (a–c) and Au/TiO₂-0 0 1 (d–f) catalysts, with gold clusters marked in yellow circles.

3.2. CO oxidation reaction catalytic performances

The CO oxidation reaction were used to value these two catalysts and the light-off reactivity based on equal catalyst weights was shown in Fig. 2a, where the Au/TiO₂-1 0 1 catalyst performed much better than Au/TiO₂-0 0 1. Basically, the Au/TiO₂-1 0 1 catalyst exhibits almost 9 times higher CO conversion (70% vs. 8%) compared to Au/TiO₂-0 0 1 during steady test at room temperature (Fig. 2b). Furthermore, the Au/TiO₂-1 0 1 catalyst still exhibited high CO conversion of 59% at lower temperature of 0 °C with a very high GHSV (GHSV = 200,000 mL·h⁻¹g_{cat}⁻¹), while no detectable reactivity was obtained for Au/TiO₂-0 0 1 catalyst (Fig. S7b). According to the previous research [12,47–50], the accumulation of carbonate species and the growth of gold nanoparticles which were shown in the following characterization might lead to the deactivation of Au/TiO₂ catalysts.

The activation energy (E_a) of Au/TiO₂-0 0 1 (34.0 kJ·mol⁻¹) was slightly higher than that of Au/TiO₂-1 0 1 (27.5 kJ·mol⁻¹) (Fig. 2c). Taking into account the kinetic condition, the reactivity per gram of gold for the catalysts with different well-defined terminations was calculated under the low CO conversion (5–15%) (Fig. 2d). Correspondingly, the CO converted rate of Au on TiO₂-1 0 1 surface was 15 times higher than that on the TiO₂-0 0 1 surface at 30 °C (9.33×10^{-3} mol_{CO}·Au⁻¹ s⁻¹ vs. 6.23×10^{-4} mol_{CO}·Au⁻¹ s⁻¹). After steady test, the gold particles in Au/TiO₂-1 0 1 slightly sintered from 2.2 nm to 2.9 nm (Figs. 1 and 3) coupling with the CO conversion negligible decrease from 75% to 70% after 12 h (Fig. 2b). As for the Au/TiO₂-0 0 1 catalyst, the STEM image clearly verified the proportion of ultra-small gold clusters remarkably decreased after reaction and then approach an average size of 3.5 nm (Fig. 3e, f and Fig. S8). Furthermore, the CO turnover frequency on the basis of the surface Au sites was compare based on the averaged size of Au particles after reaction (Fig. 3c and f). The estimated TOF value of Au/TiO₂-1 0 1 (2.18×10^{-2} s⁻¹) was 13.1 times higher than

Au/TiO₂-0 0 1 (1.66×10^{-3} s⁻¹) also in kinetic region. On account of the insignificant difference in the number of exposed fraction (0.427 vs. 0.374) [51], it was clearly demonstrated that the large gap (13.1 times) in activity of gold nanoparticles on the two surface ({1 0 1} > {0 0 1}) of TiO₂ were induced by intrinsic distinction of catalysts.

According to the previous reports, the size of Au nanoparticles was greatly influenced the catalytic behavior of Au catalysts for CO oxidation [50,52,53]. Delgass et al. reported that the Au nanoparticles with size ranged from 2 to 5 nm performed the highest activity in catalyzing CO oxidation among a series of Au/TS-1 catalysts [50]. Louis et al. found that Au nanoparticles with size of 2 nm showed the maximum activity of Au/TiO₂ catalysts [52]. Li et al. indicated that the Au nanoparticles on Au/TiO₂ catalyst with mean size of 3.8 nm showed the best catalytic performance for CO oxidation [53]. Furthermore, much work has been done to reveal the contribution of gold clusters to activity [7,54,55]. Hutchings et al. indicated that the bilayer clusters with diameter of ~0.5 nm showed the high catalytic activity for carbon monoxide oxidation [54]. Schroeder et al. found that metallic gold clusters on TiO₂ formed activated gold-oxygen complexes, which might play a role in the mechanism of O₂ activation and hence CO oxidation [55]. However, the previous work by our group showed that among three pure gold species (atoms, clusters and particles) supported on the same type of ceria matrix, the highly reduced Au⁰ structure in particles had the highest reactivity for CO oxidation reaction than single atoms and clusters due to the strongest ability of CO adsorption [7]. Therefore there are plenty of debates on the contribution of gold species to CO oxidation activity for CO oxidation even at Au/TiO₂ system.

Here, it was unable to compare the activity of gold clusters and particles in Au/TiO₂ system because pure gold clusters were difficult to synthesize by general deposition precipitation method [56–58]. If the activity of supported gold clusters was high, the

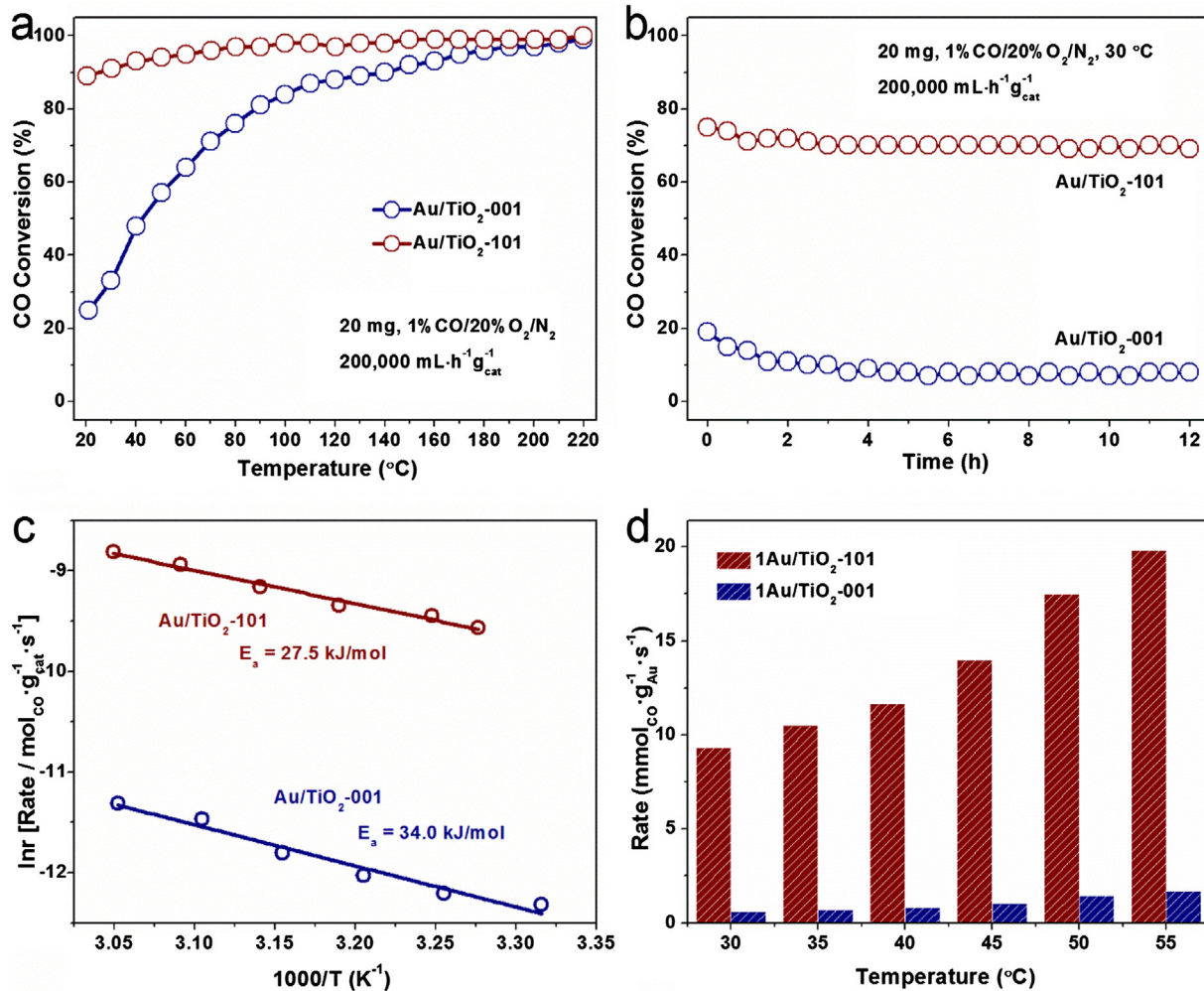


Fig. 2. The catalytic performance of gold-titanium catalysts: (a) light-off test, (b) steady-state test at a constant temperature of 30 °C, (c) the activation energy and (d) comparison of CO conversion rate over 1Au/TiO₂-0 0 1 and 1Au/TiO₂-1 0 1.

reactivity of Au/TiO₂-0 0 1 ought to be higher than that of Au/TiO₂-1 0 1. However, the above reactivity results (Fig. 2 and Fig. S7) clearly demonstrated that the Au/TiO₂-0 0 1 equipped with gold particles and ultra-small gold clusters performed lower activity in catalyzing CO oxidation reaction. Moreover, the morphology of the used catalysts collected after steady-state test was characterized by TEM (Fig. 3 and Fig. S8). Owing to the mild reaction condition, as shown in the TEM images, the geometric structure of supports was well-preserved. Similarly, the XRD patterns (Fig. S9) exhibited the same diffracted peaks of tetragonal anatase with activated samples (Fig. S2b). Thus, based on above results, we can reasonably speculate the difference between two catalysts were surface structure dependence.

3.3. Oxygen activation

To understand the origin of such differences here, the catalytic behavior should be investigated in three steps, O₂ activation, CO adsorption and CO₂ desorption. For O₂ activation, *in-situ* Raman measurement was employed to monitor the evolution of surface O on the two catalysts (Fig. 4), because Raman was sensitive to surface O vacancies. Six Raman active modes were in anatase: A_{1g} (516 cm⁻¹, symmetric stretching vibration of O—Ti—O), 2B_{1g} (397, 519 cm⁻¹, symmetric bending vibration of O—Ti—O)

and 3E_g (149, 197 and 641 cm⁻¹, antisymmetric bending vibration of O—Ti—O in TiO₂) [46,59,60]. Moreover, A_{1g} (516 cm⁻¹) and one of the B_{1g} (519 cm⁻¹) peaks were nearby and difficult to distinguish [59,60]. As proved before, the higher the fraction of exposed {001} facets was, the much stronger A_{1g} and B_{1g} peaks and much lower E_g (641 cm⁻¹) peaks was, according to experimental results and theoretical analysis [46]. Therefore, the greatly different relative intensity of various bands *in-situ* proved the crystal plane were well preserved during realistic reaction condition, which was well in line with the stable diffracted feature collected under CO oxidation reaction condition. In addition, for both catalysts, the E_g band in Raman spectra closely related to the oxygen vacancies were centered at the same values, indicating the equal number of surface oxygen vacancies [61,62]. The results from *ex-situ* Raman spectra (Fig. S10) were well in line with *in-situ* Raman. Based on previous reports, the role of oxygen vacancies on supports in activating oxygen was extremely proved, where the O₂ molecules were adsorbed and dissociated on the surface O vacancies, then was transferred to react with adsorbed CO molecules [63–65].

In addition, the *in-situ* DRIFTS-MS spectra from saturated O₂ pre-adsorption on the surface of both Au/TiO₂ catalysts to CO feed were collected as a function of evolved time. The amount of surface active O₂ molecular could be qualitatively evaluated from the generated CO₂ through surface reaction with CO molecules. As shown

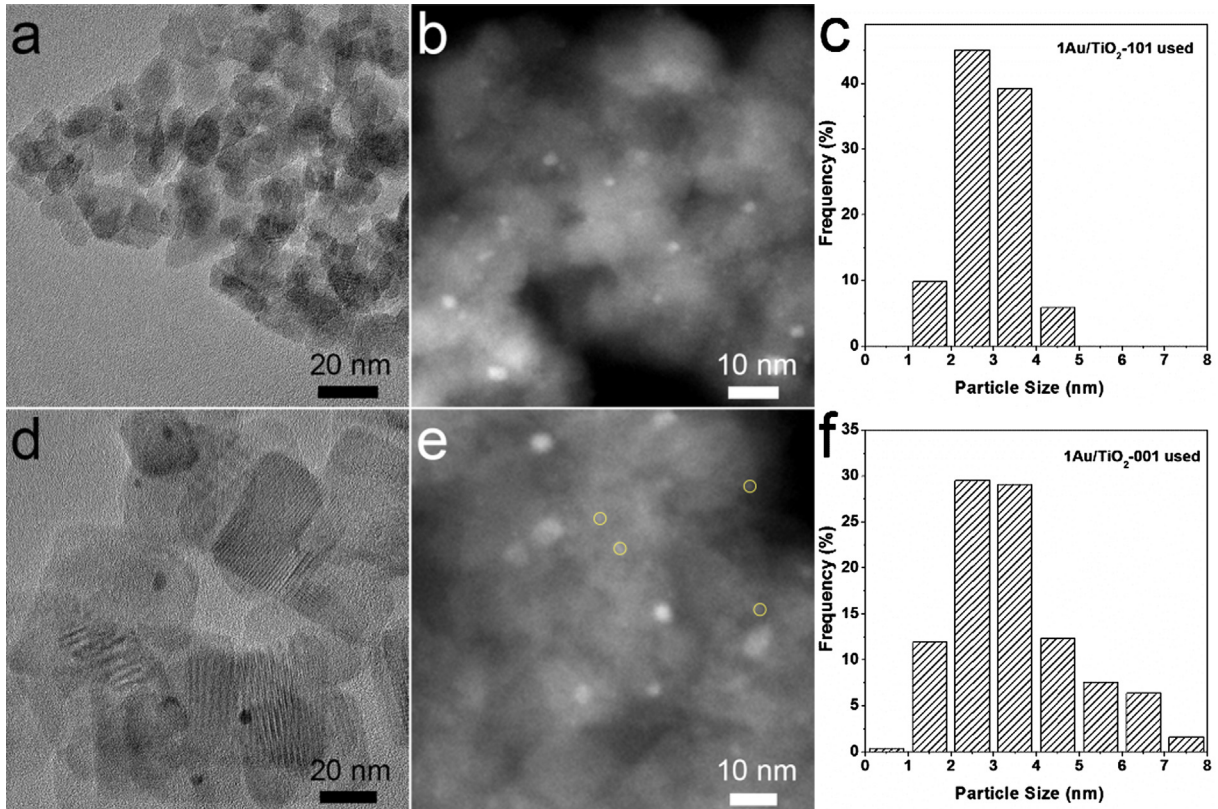


Fig. 3. TEM (a and d) and HAADF-STEM (b and e) images and size distribution (c and f) for the used Au/TiO₂-1 0 1 (a–c) and Au/TiO₂-0 0 1 (d–f) catalysts, with gold clusters marked in yellow circles.

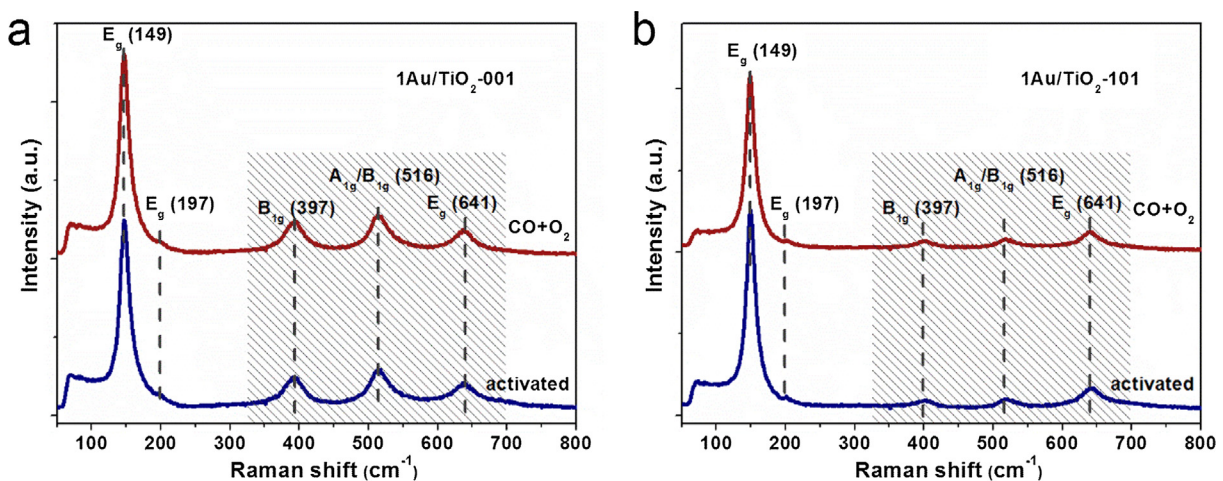


Fig. 4. *In-situ* Raman spectra of the Au/TiO₂-0 0 1 (a) and Au/TiO₂-1 0 1 (b) catalysts during reaction conditions at 30 °C.

in the DRIFTS spectra (Fig. 5a and b, Fig. S11), the evolution of produced gaseous CO₂ between 2400 and 2300 cm⁻¹ were almost the same for these two catalysts after CO injection [7,8,49]. Correspondingly, comparable CO₂ response (*m/z* = 44) was also observed by the on-line MS analysis (Fig. 5c). This fact revealed that in the course of O₂ activation during the initial period, TiO₂ {0 0 1} and {1 0 1} has little difference in the amount of surface active O₂ species at room temperature, which was well in line with the *in-situ* Raman (Fig. 4). Furthermore, it also indicated that the ability to activate O₂ molecules should not be the determining reason for distinctly superior performance of gold nanoparticles on the TiO₂-1 0 1 surface.

3.4. CO adsorption

Besides the O₂ activation, the adsorption of the other reactant, CO molecules, was also crucial for the catalytic activity. As shown in Fig. 5a and b, adsorbed CO bands centered at 2107 and 2102 cm⁻¹ were observed for Au/TiO₂-0 0 1 and Au/TiO₂-1 0 1 respectively. The absorption bands of two catalysts were closed to CO on Au⁰ sites of ~2107 cm⁻¹, basically proving the metallic nature of both gold species [7,8,45,49,66], which was in line with the XPS results (Fig. S5a) and the metallic gold was considered as active sites for CO oxidation reaction on the basis of previous researches [7,8]. However, comparing with $\nu(\text{CO})$ feature observed

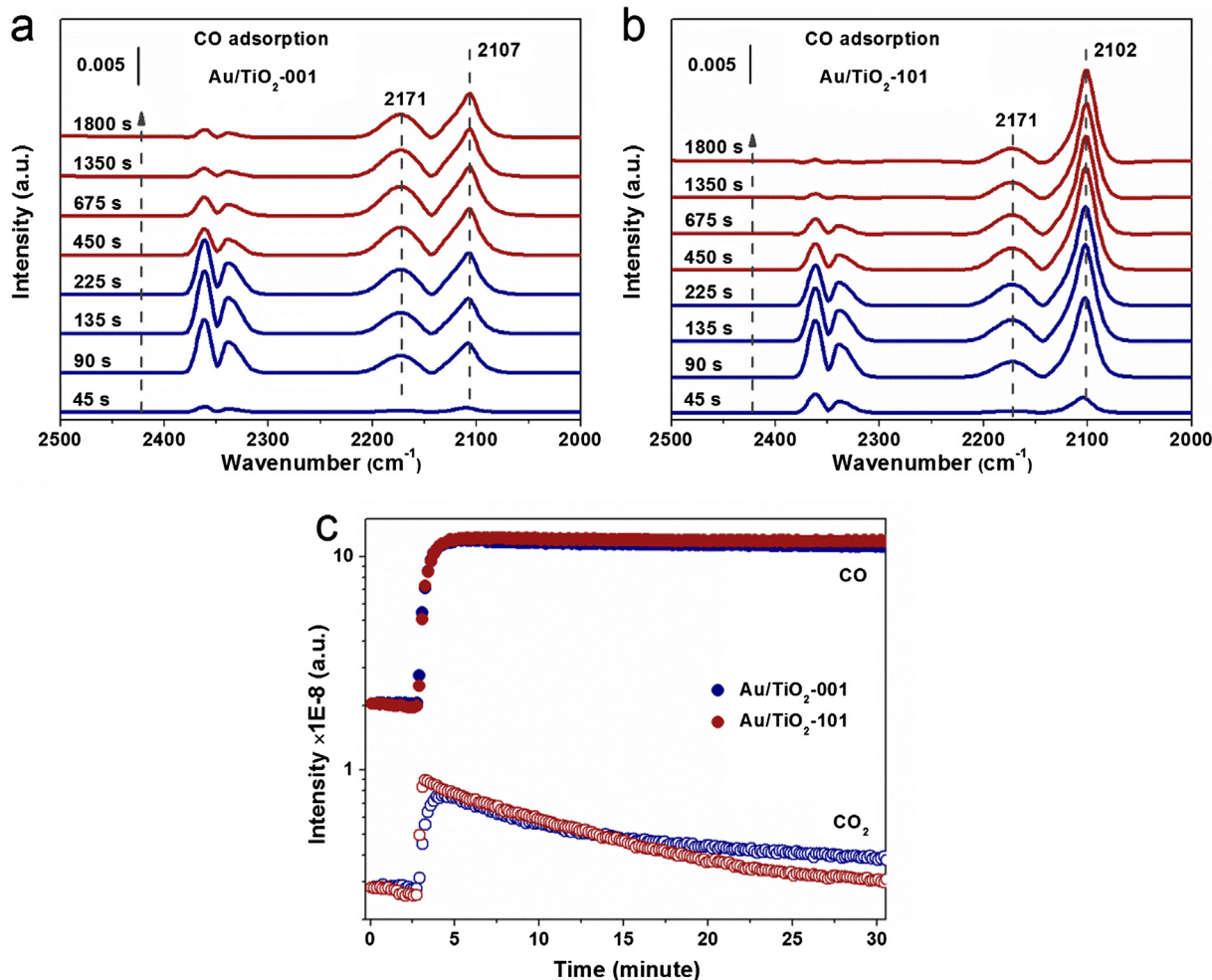


Fig. 5. *In-situ* DRIFTS-MS study of CO adsorption at 30 °C on $\text{Au}/\text{TiO}_2\text{-}0\ 0\ 1$ (a), $\text{Au}/\text{TiO}_2\text{-}1\ 0\ 1$ (b) and the corresponding MS signal (c).

at 2102 cm^{-1} for $\text{Au}/\text{TiO}_2\text{-}1\ 0\ 1$, the CO-Au absorbance signal was detected at slightly higher frequency of 2107 cm^{-1} for $\text{Au}/\text{TiO}_2\text{-}0\ 0\ 1$. It was likely the character of partial positive state of gold for $\text{Au}/\text{TiO}_2\text{-}0\ 0\ 1$ which were due to the existing of clusters according to the TEM results (Fig. 1e) [7,66].

On the other hand, the behavior of CO adsorption on the complex catalysts was also experimentally and computationally

valued. The disparity of spectral intensity, as shown in Fig. 6a, indicated that the metallic gold on $\text{Au}/\text{TiO}_2\text{-}1\ 0\ 1$ is a better chemisorption media for CO than that on $\text{Au}/\text{TiO}_2\text{-}0\ 0\ 1$. The adsorption energies of CO molecules onto Au sites of the $\text{Au}/\text{TiO}_2\text{-}0\ 0\ 1$ and $\text{Au}/\text{TiO}_2\text{-}1\ 0\ 1$ catalysts were theoretically calculated separately (Fig. 6b and Fig. S12). An 11 atoms gold cluster adsorbed on TiO_2 was selected as the substrate model for DFT calculation. A total

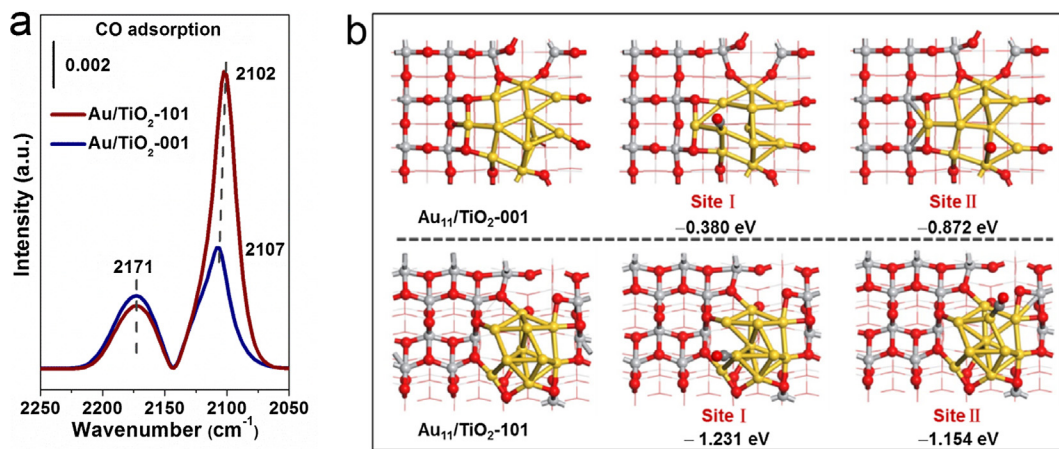


Fig. 6. *In-situ* DRIFTS spectra of CO adsorption at 30 °C on the $\text{Au}/\text{TiO}_2\text{-}0\ 0\ 1$ and $\text{Au}/\text{TiO}_2\text{-}1\ 0\ 1$ catalysts at 450 s (a), calculated CO adsorption sites and adsorption energies (b). Red balls: O atoms, light gray balls: Ti atoms, dark gray balls: C atoms and yellow balls: Au atoms.

Table 1

Calculated CO adsorption energies of the Au/TiO₂-0 0 1 and Au/TiO₂-1 0 1 catalysts.

Au ₁₁ /TiO ₂ -0 0 1		Au ₁₁ /TiO ₂ -1 0 1	
Site [*]	Adsorption energy (eV)	Site [*]	Adsorption energy (eV)
I	-0.380	I	-1.231
II	-0.872	II	-1.154
III	-0.780	III	-1.267
IV	-1.221	IV	-1.297
V	-1.987	V	-1.425
VI	-0.717	VI	-2.109
VII	-1.365	VII	-1.489
VIII	-1.329	VIII	-1.759
IX	-2.361	IX	-1.516
X	-1.441	X	—

* All the adsorption sites are top-conformations, i.e. CO bonding with one Au atom; I, II and III stand for Au–Au–CO adsorption structures, while other sites present the O–Au–CO.

of 10 Au atoms were exposed on the surface of Au₁₁/TiO₂-0 0 1. Three of them were located in the surface layer, which was only formed Au–Au bonds. The remaining seven atoms were at the interface between gold cluster and TiO₂, that is, Au–O bonds were formed on these 7 atoms. The combination between clusters and TiO₂-1 0 1 was similar to that of TiO₂-0 0 1. There were three surface gold atoms and six interfaces gold atoms when two atoms

were hid in the bulk and could not adsorb CO. The energy of CO adsorbed on each gold atom at different positions was calculated by the first principle method (Table 1). For ease comparison,

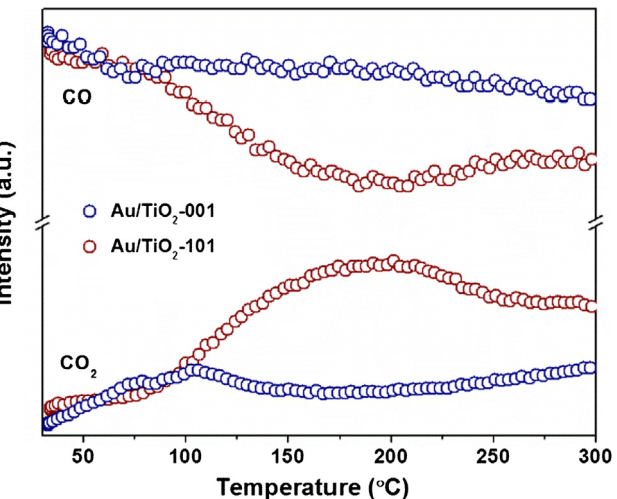


Fig. 8. CO-TPR profiles of the Au/TiO₂-0 0 1 and Au/TiO₂-1 0 1 catalysts.

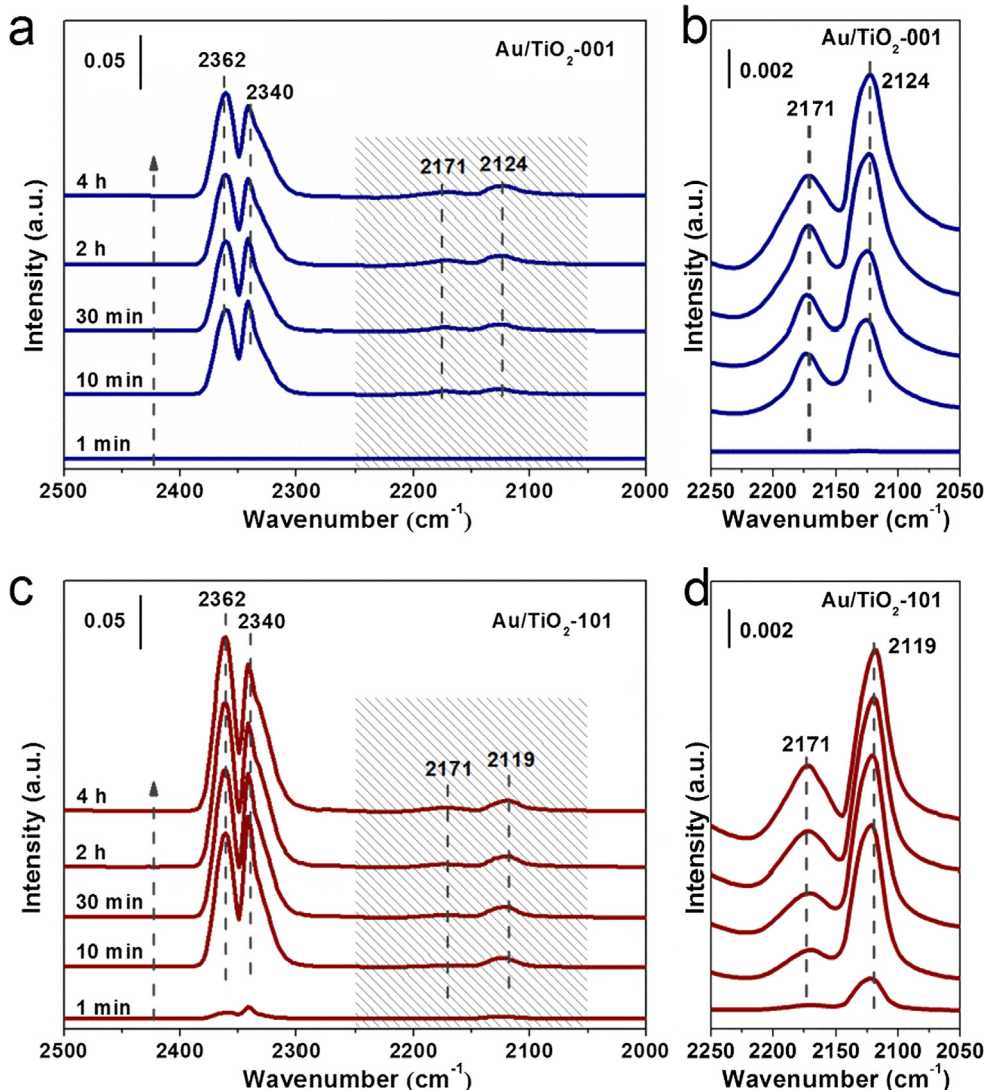


Fig. 7. In-situ DRIFTS spectra of C=O region for Au/TiO₂-0 0 1 (a and b) and Au/TiO₂-1 0 1 (c and d) catalysts during steady-state test at 30 °C.

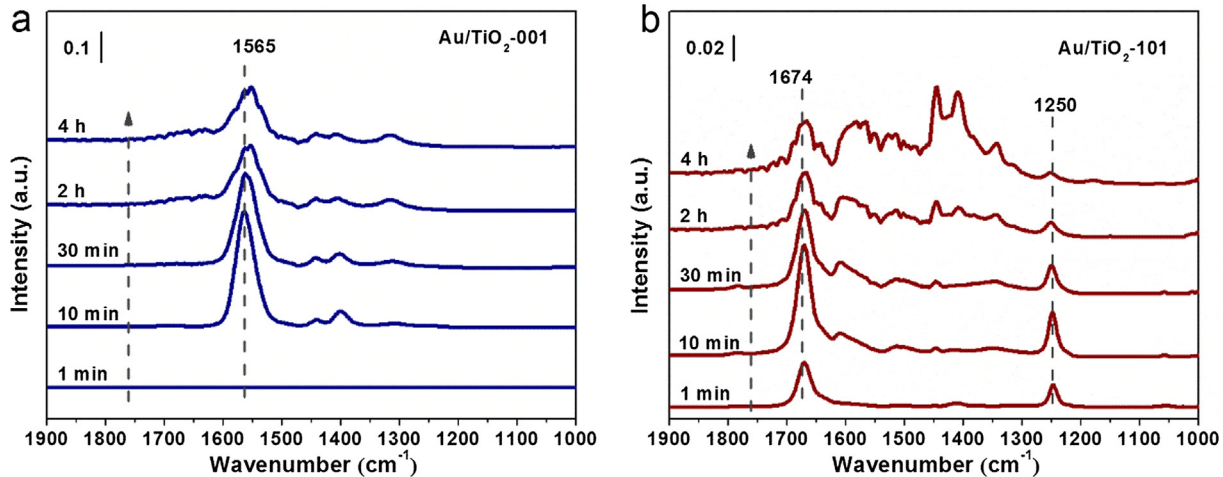


Fig. 9. *In-situ* DRIFTS spectra of carbonate region (1900–1000 cm⁻¹) for Au/TiO₂-0 01 (a) and Au/TiO₂-1 01 (b) catalysts under steady-state test at 30 °C.

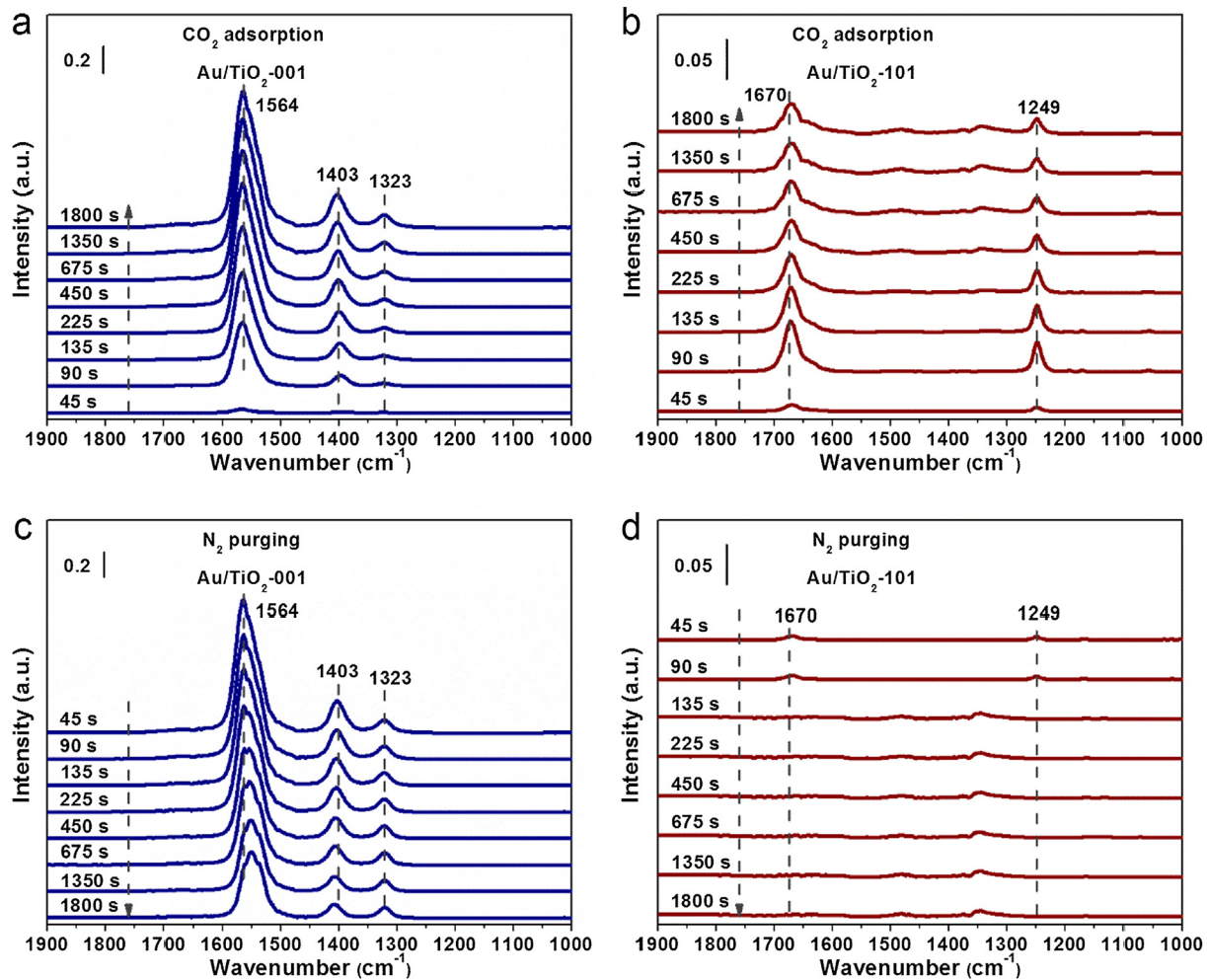


Fig. 10. *In-situ* DRIFTS study of CO₂ adsorption (a and b) and N₂ purging (c and d) on Au/TiO₂-0 01 (a and c) and Au/TiO₂-1 01 (b and d) at 30 °C.

all the adsorption sites were top-conformations. Because the gold particles in catalysts we prepared were much bigger than Au₁₁ which were the model for calculation, the CO adsorption on surface gold atoms (site I, site II, site III) was more reliable to reflect the ability of adsorption for real catalysts. Obviously, CO was preferred to adsorb on the metallic gold sites in Au₁₁/TiO₂-1 01 than

that in Au₁₁/TiO₂-0 01 (site I: -1.231 eV vs. -0.380 eV; site II: -1.154 eV vs. -0.872 eV; site III: -1.267 eV vs. -0.380 eV). These simulated calculation results well matched with the results of CO adsorption from *in-situ* DRIFTS results above (Fig. 6a), proving the superior CO adsorption ability of Au nanoparticles on TiO₂-1 01 than TiO₂-0 01.

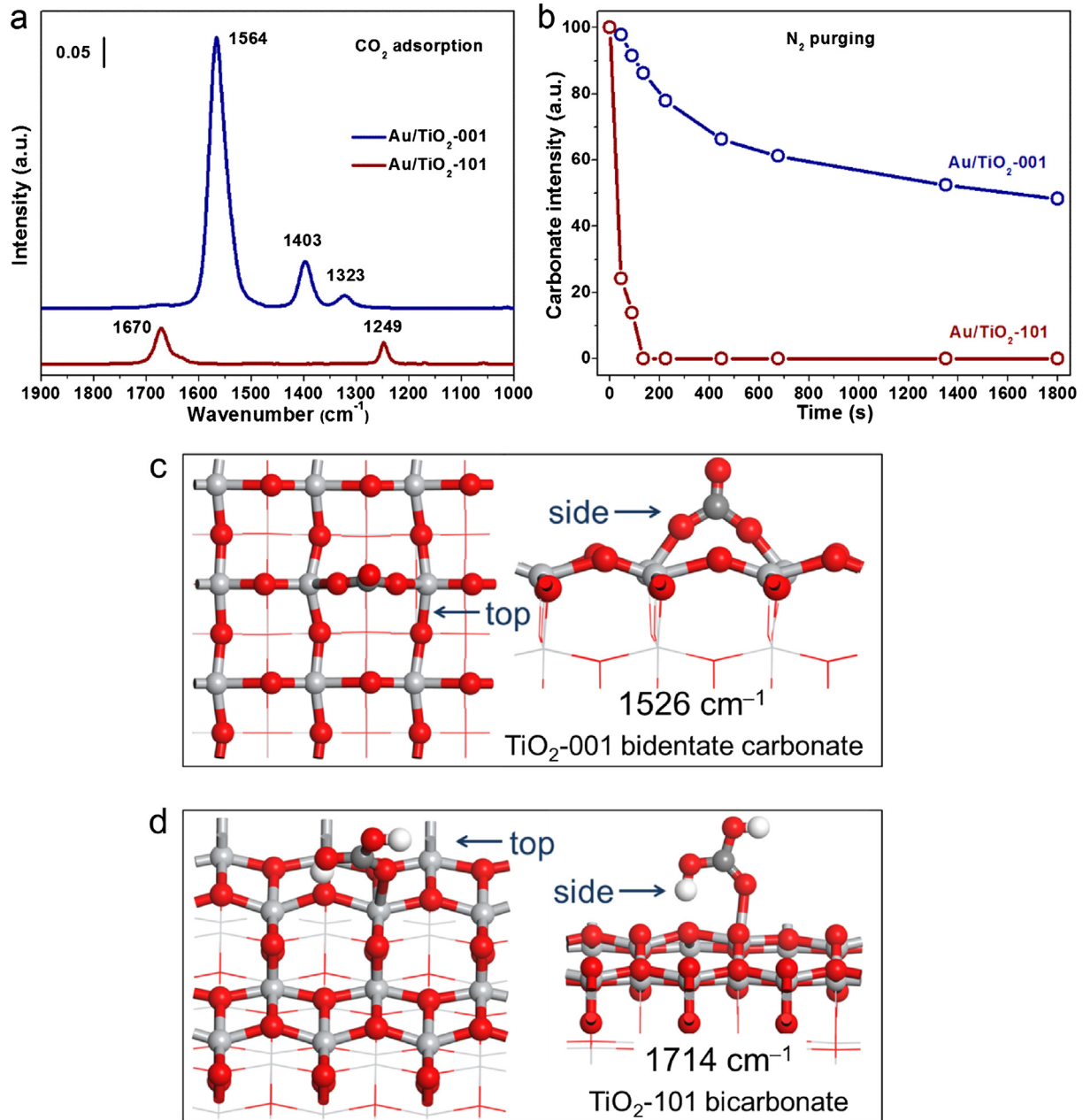


Fig. 11. *In-situ* DRIFTS study of CO_2 adsorption (a), the intensity of carbonate species during N_2 purging with the function of time (b) and the calculated carbonate species of the $\text{Au/TiO}_2\text{-0 0 1}$ (c) and $\text{Au/TiO}_2\text{-1 0 1}$ (d) catalysts on the top and side view.

To further investigate the relation between gold species and reactivity during CO oxidation reaction, the *in-situ* DRIFTS with steady-state test mode was performed (Fig. 7). For ease comparison, the CO region (2250 cm^{-1} – 2050 cm^{-1}) was magnified (Fig. 7b and d). When switching to reaction gas, the CO adsorption bands centered at 2124 cm^{-1} and 2119 cm^{-1} were observed for $\text{Au/TiO}_2\text{-0 0 1}$ and $\text{Au/TiO}_2\text{-1 0 1}$, respectively. Compared with CO adsorption experiments and steady-state test, the peaks of CO-Au^0 centered at 2107 cm^{-1} and 2102 cm^{-1} (Fig. 6a) were blue shifted to 2124 cm^{-1} and 2119 cm^{-1} , respectively. The shift was caused by the $\text{CO}-\text{Au}^{+}-\text{O}^{2-}$ interactions as a result of CO adsorption on Au^0 [67,68]. Moreover, the CO_2 signal centered between 2400 and 2300 cm^{-1} were observed during the steady-state test for these two samples. The gaseous CO_2 signal for $\text{Au/TiO}_2\text{-1 0 1}$ was much higher than $\text{Au/TiO}_2\text{-0 0 1}$, indicating a higher CO oxidation reactivity for $\text{Au/TiO}_2\text{-1 0 1}$ than that for $\text{Au/TiO}_2\text{-0 0 1}$ which

was corresponding to the results of activity (Fig. 2). Both CO adsorption and steady-state test indicated that crystal plane affect the gold status due to distinct interaction between support with different crystal plane and gold. The different behavior of CO adsorption was also confirmed by CO-TPR (Fig. 8). The larger CO_2 peak in $\text{Au/TiO}_2\text{-1 0 1}$ was owing to the much more efficient CO-Au^0 species and more active oxygen species which can react with CO at high temperature.

3.5. CO_2 desorption

Apart from the O_2 activation and the efficiency of CO adsorption, desorption of products was also significant for the resulting catalytic reactivity. The role of carbonates accumulation for the Au/TiO_2 catalysts during steady-state test was further studied. As shown in Fig. 9, different carbonate species appeared during

steady-state test for two catalysts. As for Au/TiO₂-0 0 1, the band centered at 1565 cm⁻¹ was the dominant carbonate species which was signed to bidentate carbonate [18,69]. Oppositely, the bands centered at 1674 cm⁻¹ and 1250 cm⁻¹ were the dominant carbonate species which were signed to bicarbonate for Au/TiO₂-1 0 1 [18,69]. Except the diversity of carbonate species, the intensity was in great difference for two catalysts with Au/TiO₂-0 0 1 higher than Au/TiO₂-1 0 1, indicating the strongly adsorption of carbonate species on Au/TiO₂-0 0 1. Therefore, the carbonate accumulation influenced by crystal plane effect could be another reason for the lower reactivity of Au/TiO₂-0 0 1.

In-situ DRIFTS analysis of CO₂ adsorption-desorption (Figs. 10 and 11) and CO₂-TPD (Fig. 12) were carried out to further investigate the behavior of carbonate. The CO₂ adsorption experiment (Fig. 10) obtained the similar results with steady-state test. For ease to compare, two CO₂ adsorption spectra were selected from two catalysts, respectively, and put together in Fig. 11a. When injecting CO₂, bidentate carbonate species (1564 cm⁻¹ and 1323 cm⁻¹) were appeared on Au/TiO₂-0 0 1 demonstrating that the adsorbed CO₂ converted to carbonate species which attached tightly on the surface of catalysts and hindered the active site resulting in the lower reactivity. The band at 1403 cm⁻¹ was corresponding to bridged carbonate [18]. In contrast, the intensity of bicarbonate (1670 cm⁻¹ and 1249 cm⁻¹) on the Au/TiO₂-1 0 1 was weaker than the intensity of bidentate carbonate on the Au/TiO₂-0 0 1. When N₂ purging (Fig. 10b and d for original spectra and Fig. 11b for intensity of carbonate vary with the change of N₂ purging time), the carbonate on Au/TiO₂-1 0 1 was disappeared after 135 s purging, however, the carbonate still remaining 48% on Au/TiO₂-0 0 1. The results indicated that the adsorbed carbonate on Au/TiO₂-0 0 1 was much stronger and more difficult to desorb than that on Au/TiO₂-1 0 1 which could be a reason for the lower reactivity of Au/TiO₂-0 0 1.

The structure of carbonate species on two TiO₂ surfaces was calculated by DFT (Fig. 11c and d). As for TiO₂-0 0 1, the angle of surface atoms (\angle TiOTi) was 149.4° and the distance between two adjacent titanium atoms was 3.782 Å. Considering that the coordination number of surface titanium atoms was five, CO₂ molecules could adsorb on this unsaturated Ti atoms. Once the Ti atom bonded with CO₂, the Ti—O bond ruptured and CO₃²⁻ was formed. As for stereo-chemical configuration, the angle of \angle TiOC was 155.1° and 164.0°, while the angle of \angle OCO was 113.7°. Moreover, the Ti—O bond between surface and CO₃²⁻ were 1.859 Å and 1.832 Å, while C—O bond were 1.351 Å and 1.337 Å. The aforementioned data indicated that the combination between

CO₃²⁻ and TiO₂-0 0 1 with O-defect was geometric favorable, therefore the formation process was a representative exothermic reaction, -0.864 eV. However, as for TiO₂-1 0 1, the carbonate can only form a Ti—O—C—O tetra-atomic ring after the formation of CO₃²⁻. The tension of tetra-atomic ring was reduced the bonding stability, and the corresponding energy change was -0.129 eV. Therefore, carbonate was relatively easy to form on the TiO₂-0 0 1 and bicarbonate was facile formed on the TiO₂-1 0 1. The vibrational frequencies of simulated catalysts were obtained from DFT calculations, while the only two conformations (Fig. 11c and d) had analogous infrared wave numbers (less than 3%), i.e. bidentate carbonate structure of TiO₂-0 0 1, 1526 cm⁻¹ vs. 1564 cm⁻¹; bicarbonate structure of TiO₂-1 0 1, 1714 cm⁻¹ vs. 1670 cm⁻¹.

As for CO₂-TPD (Fig. 12), hardly any peaks were shown for Au/TiO₂-1 0 1 and TiO₂-1 0 1 indicating the weak CO₂ adsorption. However, large peak centered at 74.5 °C was shown for TiO₂-0 0 1 and peak centered at 108.9 °C and a shoulder peak at 64.4 °C were shown for Au/TiO₂-0 0 1 suggesting the strong CO₂ adsorption which were consisted with the results of *in-situ* DRIFTS for CO₂ adsorption and desorption.

4. Conclusions

In summary, we successfully prepared Au/TiO₂ catalysts with different TiO₂ crystal plane by DP method to investigate the influence of CO adsorption and CO₂ desorption on reactivity in catalyzing CO oxidation. Obviously, the reactivity of Au/TiO₂-1 0 1 was higher than Au/TiO₂-0 0 1. It was proved that gold particles were in Au/TiO₂-1 0 1 while not only gold particles but also clusters were in Au/TiO₂-0 0 1 due to the different interaction between gold and supports exposed distinct crystal plane. Combining *in-situ* DRIFTS measurement and theoretical calculation, we concluded that CO was more effectively adsorbed on Au⁰ in Au/TiO₂-1 0 1 than that in Au/TiO₂-0 0 1. Furthermore, during CO oxidation reaction, the obtained carbonate species were more tightly adsorbed and more difficult to desorb on Au/TiO₂-0 0 1 than on Au/TiO₂-1 0 1 after the reaction production CO₂ adsorbed on the surface of catalysts. The much stronger adsorbed carbonate species which hindered the active site may also result in lower reactivity of Au/TiO₂-0 0 1. Finally, we illustrated that the efficiency of CO adsorption and CO₂ desorption for Au/TiO₂ system displayed enormous effects on catalytic activity during CO oxidation reaction.

Acknowledgement

This work is financially supported from the Excellent Young Scientists Fund from National Science Foundation of China (NSFC) (grant no. 21622106), other projects from the NSFC (grant nos. 21805167 and 21771117), the Outstanding Scholar Fund (grant no. JQ201703) and the Doctoral Fund (grant no. ZR2018BB010) from the Science Foundation of Shandong Province of China and the Taishan Scholar Project of Shandong Province of China. We thank the Center of Structural Characterization and Property Measurements at Shandong University for the help on sample characterizations.

Appendix A. Supplementary material

Supplementary data to this article can be found online at <https://doi.org/10.1016/j.jcat.2019.06.038>.

References

- [1] Z.R. Tang, J.K. Edwards, J.K. Bartley, S.H. Taylor, A.F. Carley, A.A. Herzing, C.J. Kiely, G.J. Hutchings, J. Catal. 249 (2007) 208.

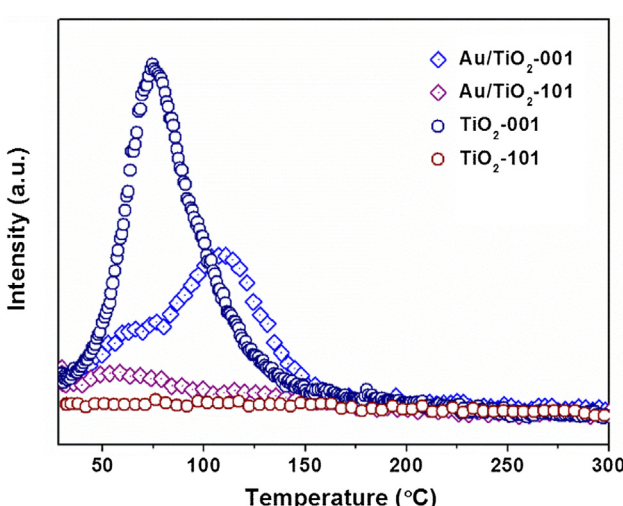


Fig. 12. CO₂-TPD profiles of TiO₂ supports and Au/TiO₂ catalysts.

- [2] M.J. Li, Z.L. Wu, Z. Ma, V. Schwartz, D.R. Mullins, S. Dai, S.H. Overbury, *J. Catal.* 266 (2009) 98.
- [3] M. Haruta, T. Kobayashi, H. Sano, N. Yamada, *Chem. Lett.* 16 (1987) 405.
- [4] Z.L. Wu, S.H. Zhou, H.G. Zhu, S. Dai, S.H. Overbury, *J. Phys. Chem. C* 113 (2009) 3726.
- [5] G.J. Hutchings, M.S. Hall, A.F. Carley, P. Landon, B.E. Solsona, C.J. Kiely, A. Herzing, M. Makkee, J.A. Moulijn, A. Overweg, J.C. Fierro-Gonzalez, J. Guzman, B.C. Gates, *J. Catal.* 242 (2006) 71–81.
- [6] I.X. Green, W. Tang, M. Neurock, J.T. Yates, *Science* 333 (2011) 736–739.
- [7] L.W. Guo, P.P. Du, X.P. Fu, C. Ma, J. Zeng, R. Si, Y.Y. Huang, C.J. Jia, Y.W. Zhang, C. H. Yan, *Nat. Commun.* 7 (2016) 13481.
- [8] S. Wei, X.P. Fu, W.W. Wang, Z. Jin, Q.S. Song, C.J. Jia, *J. Phys. Chem. C* 122 (2018) 4928.
- [9] X.J. Wei, B. Shao, Y. Zhou, Y. Li, C.C. Jin, J.Y. Liu, W.J. Shen, *Angew. Chem. Int. Ed.* 57 (2018) 11289.
- [10] S.H. Overbury, L. Ortiz-Soto, H. Zhu, B. Lee, M.D. Amiridis, S. Dai, *Catal. Lett.* 95 (2004) 99.
- [11] H.L. Tang, F. Liu, J.K. Wei, B.T. Qiao, K.F. Zhao, Y. Su, C.Z. Jin, L. Li, J.Y. Liu, J.H. Wang, T. Zhang, *Angew. Chem. Int. Ed.* 55 (2016) 10606.
- [12] Y. Wang, D. Widmann, R.J. Behm, *ACS Catal.* 7 (2017) 2339.
- [13] H.L. Tang, J.K. Wei, F. Liu, B.T. Qiao, X.L. Pan, L. Li, J.Y. Liu, J.H. Wang, T. Zhang, *J. Am. Chem. Soc.* 138 (2016) 56.
- [14] Y.C. Wang, D. Widmann, F. Lehnert, D. Gu, F. Schüth, R.J. Behm, *Angew. Chem. Int. Ed.* 56 (2017) 1.
- [15] T.A. Ntho, J.A. Anderson, M.S. Scurrell, *J. Catal.* 261 (2009) 94.
- [16] C.W. Yang, X.J. Yu, S. Heißler, A. Nefedov, S. Colussi, J. Llorca, A. Trovarelli, Y. Wang, C. Woll, *Angew. Chem. Int. Ed.* 56 (2017) 375.
- [17] L. Mino, G. Spoto, A.M. Ferrari, *J. Phys. Chem. C* 118 (2014) 25016.
- [18] S.L. Chen, T. Cao, Y.X. Gao, D. Li, F. Xiong, W.X. Huang, *J. Phys. Chem. C* 120 (2016) 21472.
- [19] X. Zhang, H. Wang, B.Q. Xu, *J. Phys. Chem. B* 109 (2005) 9678.
- [20] C.J. Jia, Y. Liu, H. Bongard, F. Schüth, *J. Am. Chem. Soc.* 132 (2010) 1520.
- [21] Y. Guo, D. Gu, Z. Jin, P.P. Du, R. Si, J. Tao, W.Q. Xu, Y.Y. Huang, S. Senanayake, Q. S. Song, C.J. Jia, F. Schüth, *Nanoscale* 7 (2015) 4920.
- [22] Y.X. Liu, H.X. Dai, J.G. Deng, S.H. Xie, H.G. Yang, W. Tan, W. Han, Y. Jiang, G.S. Guo, *J. Catal.* 309 (2014) 408.
- [23] M.M. Schubert, S. Hackenberg, A.C. van Veen, M. Muhler, V. Plzak, R.J. Behm, *J. Catal.* 197 (2001) 113.
- [24] D. Widmann, Y. Liu, F. Schüth, R.J. Behm, *J. Catal.* 276 (2010) 292.
- [25] R. Si, M. Flytzani-Stephanopoulos, *Angew. Chem. Int. Ed.* 47 (2008) 2884.
- [26] W.J. Xue, Y.F. Wang, P. Li, Z.T. Liu, Z. Hao, C.Y. Ma, *Catal. Commun.* 12 (2011) 1265.
- [27] L.C. Liu, C.Y. Ge, W.X. Zou, X.R. Gu, F. Gao, L. Dong, *Phys. Chem. Chem. Phys.* 17 (2015) 5133.
- [28] L.C. Liu, X.R. Gu, Y. Cao, X.J. Yao, L. Zhang, C.J. Tang, F. Gao, L. Dong, *ACS Catal.* 3 (2013) 2768.
- [29] Y.F. Li, U. Aschauer, J. Chen, A. Selloni, *Acc. Chem. Res.* 47 (2014) 3361.
- [30] M. Lazzeri, A. Vittadini, A. Selloni, Structure and energetics of stoichiometric TiO₂ anatase surfaces, *Phys. Rev. B* 63 (2001) 155409.
- [31] Y. Liang, S.P. Gan, S.A. Chambers, *Phys. Rev. B* 63 (2001) 235402.
- [32] B. Schumacher, Y. Denkowitz, V. Plzak, M. Kinne, R.J. Behm, *J. Catal.* 224 (2004) 449.
- [33] M. McEntee, A. Stevanovic, W. Tang, M. Neurock, J.T. Yates, *J. Am. Chem. Soc.* 137 (2015) 1972.
- [34] F. Bocuzzi, A. Chiorino, M. Manzoli, P. Lu, T. Akita, S. Ichikawa, M. Haruta, *J. Catal.* 202 (2001) 256.
- [35] D. Li, S.L. Chen, R. You, Y.X. Liu, M. Yang, T. Cao, K. Qian, Z.H. Zhang, J. Tian, W.X. Huang, *J. Catal.* 368 (2018) 163.
- [36] L.C. Liu, X.R. Gu, Z.Y. Ji, W.X. Zou, C.J. Tang, F. Gao, L. Dong, *J. Phys. Chem. C* 117 (2013) 18578.
- [37] X.G. Han, Q. Kuang, M.S. Jin, Z.X. Xie, L.S. Zheng, *J. Am. Chem. Soc.* 131 (2009) 3152.
- [38] G. Kresse, J. Hafner, *Phys. Rev. B* 47 (1993) 558.
- [39] G. Kresse, J. Furthmüller, *Phys. Rev. B* 54 (1996) 11169.
- [40] G. Kresse, J. Hafner, *Phys. Rev. B* 49 (1994) 14251.
- [41] G. Kresse, D. Joubert, *Phys. Rev. B* 59 (1999) 1758.
- [42] J.P. Perdew, K. Burke, M. Ernzerhof, *Phys. Rev. Lett.* 77 (1996) 3865.
- [43] P.E. Blöchl, *Phys. Rev. B* 50 (1994) 17953.
- [44] Y. Ji, Y. Luo, *J. Am. Chem. Soc.* 138 (2016) 15896.
- [45] I.X. Green, W. Tang, M. McEntee, M. Neurock, J.T. Yates, *J. Am. Chem. Soc.* 134 (2012) 12717.
- [46] F. Tian, Y.P. Zhang, J. Zhang, C.X. Pan, *J. Phys. Chem. C* 116 (2012) 7515.
- [47] M.G. Mendez-Medrano, E. Kowalska, A. Lehoux, A. Herissan, B. Ohtani, S. Rau, C. Colbeau-Justin, J.L. Rodriguez-Lopez, H. Remita, *J. Phys. Chem. C* 120 (2016) 25010.
- [48] J. Saavedra, C. Powell, B. Panthi, C.J. Pursell, B.D. Chandler, *J. Catal.* 307 (2013) 37.
- [49] Y. Denkowitz, B. Schumacher, G. Kucerová, R.J. Behm, *J. Catal.* 267 (2009) 78.
- [50] W.S. Lee, R. Zhang, M.C. Akatay, C.D. Baertsch, E.A. Stach, F.H. Ribeiro, W.N. Delgass, *ACS Catal.* 1 (2011) 1327.
- [51] M. Shekar, J. Wang, W.S. Lee, W.D. Williams, S.M. Kim, E.A. Stach, J.T. Miller, W.N. Delgass, F.H. Ribeiro, *J. Am. Chem. Soc.* 134 (2012) 4700.
- [52] R. Zanella, S. Giorgio, C.H. Shin, C.R. Henry, C. Louis, *J. Catal.* 222 (2004) 357.
- [53] M.M. Du, D.H. Sun, H.W. Yang, J.L. Huang, X.L. Jing, T. Odoom-Wubah, H.T. Wang, L.S. Jia, Q.B. Li, *J. Phys. Chem. C* 118 (2014) 19150.
- [54] A.A. Herzing, C.J. Kiely, A.F. Carley, P. Landon, G.J. Hutchings, *Science* 321 (2008) 1331.
- [55] N. Weiher, A.M. Beesley, N. Tsapatsaris, L. Delannoy, C. Louis, J.A. van Bokhoven, S.L.M. Schroeder, *J. Am. Chem. Soc.* 129 (2007) 2240.
- [56] W.C. Li, M. Comotti, F. Schüth, *J. Catal.* 237 (2006) 190.
- [57] M.C. Kung, R.J. Davis, H.H. Kung, *J. Phys. Chem. C* 111 (2007) 11767.
- [58] R. Si, J. Liu, K. Yang, X. Chen, W. Dai, X. Fu, *J. Catal.* 311 (2014) 71.
- [59] L.M. Martínez Tejada, A. Muñoz, M.A. Centeno, J.A. Odriozola, *J. Raman Spectrosc.* 47 (2016) 189.
- [60] Y. Zhang, W. Wu, K. Zhang, C.H. Liu, A.F. Yu, M.Z. Peng, J.Y. Zhai, *Phys. Chem. Chem. Phys.* 18 (2016) 32178.
- [61] J.C. Parker, R.W. Siegel, *Appl. Phys. Lett.* 51 (1990) 943.
- [62] J. Zhu, J. Ren, Y.N. Huo, Z.F. Bian, H.X. Li, *J. Phys. Chem. C* 111 (2007) 18965.
- [63] D. Widmann, R.J. Behm, *Acc. Chem. Res.* 47 (2014) 740.
- [64] D. Widmann, R.J. Behm, *Angew. Chem. Int. Ed.* 50 (2011) 1024.
- [65] S. Garrettin, Y.L. Hao, V. Aguilar-Guerrero, B.C. Gates, S. Trasobares, J.J. Calvino, A. Corma, *Eur. J. 13* (2007) 7771.
- [66] M. Mihaylov, H. Knözinger, K. Hadjivanov, B.C. Gates, *Chemie Ingenieur Technik* 79 (2007) 795.
- [67] T. Goto, T. Itoh, T. Akamatsu, N. Izu, W. Shin, *Sens. Actuators, B Chem.* 223 (2016) 774.
- [68] S.R. Wang, Y.J. Wang, J.Q. Jiang, R. Liu, M.Y. Li, Y.M. Wang, Y. Su, B.L. Zhu, S.M. Zhang, W.P. Huang, S.H. Wu, *Catal. Commun.* 10 (2009) 640.
- [69] L.J. Liu, H.L. Zhao, J.M. Andino, Y. Li, *ACS Catal.* 2 (2012) 1817.